

Instrumentation of JUNO 3-inch PMTs

Jilei Xu^{*8}, Miao He^{†8}, Cédric Cerna^{‡36}, Yongbo Huang^{§22}, Thomas Adam³⁷, Shakeel Ahmad⁵⁷, Rizwan Ahmed⁵⁷, Fengpeng An¹⁶, Costas Andreopoulos⁶⁵, Giuseppe Andronico⁴⁷, João Pedro Athayde Marcondes de André³⁷, Nikolay Anfimov⁵⁸, Vito Antonelli⁴⁹, Tatiana Antoshkina⁵⁸, Didier Auguste³⁵, Weidong Bai¹⁶, Nikita Balashov⁵⁸, Andrea Barresi⁵⁰, Davide Basilico⁴⁹, Eric Baussan³⁷, Marco Beretta⁴⁹, Antonio Bergnoli⁵², Nikita Bessonov⁵⁸, Daniel Bick⁴¹, Lukas Bieger⁴⁶, Svetlana Biktemerova⁵⁸, Thilo Birkenfeld⁴⁰, Simon Blyth⁸, Anastasia Bolshakova⁵⁸, Mathieu Bongrand³⁹, Matteo Borghesi⁵⁰, Dominique Breton³⁵, Augusto Brigatti⁴⁹, Riccardo Brugnera⁵³, Riccardo Bruno⁴⁷, Antonio Budano⁵⁶, Jose Bustos³⁸, Marcel Büchner⁴³, Anatael Cabrera³⁵, Barbara Caccianiga⁴⁹, Hao Cai²⁶, Xiao Cai⁸, Yanke Cai⁸, Zhiyan Cai⁸, Stéphane Callier³⁶, Steven Calvez³⁹, Antonio Cammi^{¶51}, Chuanya Cao⁸, Guofu Cao⁸, Jun Cao⁸, Yaoqi Cao^{66,65}, Rossella Caruso⁴⁷, Vanessa Cerrone⁵³, Jinfan Chang⁸, Yun Chang³¹, Auttakit Chatrabhuti⁶², Chao Chen⁸, Guoming Chen²², Jiahui Chen⁸, Jian Chen¹⁶, Jing Chen¹⁶, Junyou Chen²², Pingping Chen¹⁴, Shaomin Chen¹⁰, Shiqiang Chen²¹, Xin Chen^{21,8}, Yiming Chen⁸, Yixue Chen⁹, Yu Chen¹⁶, Ze Chen^{45,43}, Zhangming Chen²³, Zhiyuan Chen⁸, Jie Cheng⁹, Yaping Cheng⁷, Yu Chin Cheng³², Alexander Chepurnov⁶⁰, Alexey Chetverikov⁵⁸, Davide Chiesa⁵⁰, Pietro Chimenti³, Po-Lin Chou³⁰, Ziliang Chu⁸, Artem Chukanov⁵⁸, Gérard Claverie³⁶, Catia Clementi⁵⁴, Barbara Clerbaux², Claudio Coletta⁵⁰, Simon Csakli⁴⁴, Chenyang Cui⁸, Olivia Dalager⁶⁷, Zhi Deng¹⁰, Ziyan Deng⁸, Xiaoyu Ding²⁰, Xuefeng Ding⁸, Yayun Ding⁸, Bayu Dirgantara⁶⁴, Carsten Dittrich⁴⁴, Sergey Dmitrievsky⁵⁸, David Doerflinger⁴⁴, Dmitry Dolzhikov⁵⁸, Haojie Dong⁸, Jianmeng Dong¹⁰, Evgeny Doroshkevich⁵⁹, Marcos Dracos³⁷, Frédéric Druillolle³⁶, Ran Du⁸, Shuxian Du²⁹, Yujie Duan²⁶, Katherine Dugas⁶⁷, Stefano Dusini⁵², Hongyue Duyang²⁰, Jessica Eck⁴⁶, Timo Enqvist³⁴, Andrea Fabbri⁵⁶, Ulrike Fahrendholz⁴⁴, Lei Fan⁸, Jian Fang⁸, Wenxing Fang⁸, Elia Stanescu Farilla⁵⁶, Dmitry Fedoseev⁵⁸, Li-Cheng Feng³⁰, Qichun Feng¹⁷, Federico Ferraro⁴⁹, Daniela Fetzer⁴³, Marcellin Fozé³⁷, Amélie Fournier³⁶, Aaron Freegard²³, Feng Gao², Alberto Garfagnini⁵³, Arsenii Gavrikov⁵³, Marco Giammarchi⁴⁹, Nunzio Giudice⁴⁷, Maxim Gonchar⁵⁸, Guanghua Gong¹⁰, Hui Gong¹⁰, Yuri Gornushkin⁵⁸, Marco Grassi⁵³, Maxim Gromov⁶⁰, Vasily Gromov⁵⁸, Minhao Gu⁸, Xiaofei Gu²⁹, Yu Gu¹⁵, Mengyun Guan⁸, Yuduo Guan⁸, Nunzio Guardone⁴⁷, Rosa Maria Guizzetti⁵³, Cong Guo⁸, Wanlei Guo⁸, Caren Hagner⁴¹, Hechong Han⁸, Ran Han⁷, Yang Han¹⁶, Vidhya Thara Hariharan⁴¹, Jinhong He²⁶, Wei He⁸, Xinhai He⁸, Ziou He^{66,65}, Tobias Heinz⁴⁶, Patrick Hellmuth³⁶, Yuekun Heng⁸, YuenKeung Hor¹⁶, Shaojing Hou⁸, Yee Hsiung³², Bei-Zhen Hu⁶⁹, Hang Hu¹⁶, Jun Hu⁸, Tao Hu⁸, Yuxiang Hu⁸, Guihong Huang¹⁹, Hexiang Huang⁸, Jinhao Huang⁸, Junting Huang²³, Kaixuan Huang¹⁶, Shengheng Huang¹⁹, Tao Huang¹⁶, Xin Huang⁸, Xingtao Huang²⁰, Jiaqi Hui²³, Lei Huo¹⁷, Cédric Huss³⁶, Safeer Hussain⁵⁷, Leonard Imbert³⁹, Ara Ioannissian¹, Adrienne Jacobi⁶⁷, Arshak Jafar⁴³, Beatrice Jelmini⁵³, Xiangpan Ji²⁵, Xiaolu Ji⁸, Huihui Jia²⁵, Junji Jia²⁶, Cailian Jiang²¹, Wei Jiang⁸, Xiaoshan Jiang⁸, Xiaozhao Jiang⁸, Yijian Jiang⁹, Yixuan Jiang⁸, Xiaoping Jing⁸, Cécile Jollet³⁶, Li Kang¹⁴,

Rebin Karaparabil³⁷, Narine Kazarian¹, Ali Khan⁵⁷, Amina Khatun^{2,61}, Khanchai Khosonthongkee⁶⁴, Denis Korablev⁵⁸, Konstantin Kouzakov⁶⁰, Alexey Krasnoperov⁵⁸, Sergey Kuleshov⁵, Sindhuja Kumaran⁶⁷, Nikolay Kutovskiy⁵⁸, Loïc Labit³⁶, Tobias Lachenmaier⁴⁶, Haojing Lai²³, Cecilia Landini⁴⁹, Lorenzo Lastrucci⁵², Sébastien Leblanc³⁶, Matthieu Lecocq³⁶, Frederic Lefevre³⁹, Ruiting Lei¹⁴, Rupert Leitner³³, Jason Leung³⁰, Demin Li²⁹, Fei Li⁸, Fule Li¹⁰, Gaosong Li⁸, Hongjian Li⁸, Huang Li⁸, Jiajun Li¹⁶, Min Li³⁷, Nan Li¹², Qingjiang Li¹², Ruhui Li⁸, Rui Li²³, Shanfeng Li¹⁴, Tao Li¹⁶, Teng Li²⁰, Weidong Li^{8,11}, Xiaonan Li⁸, Yi Li¹⁴, Yichen Li⁸, Yifan Li⁸, Yufeng Li⁸, Zhaohan Li⁸, Zhibing Li¹⁶, Zi-Ming Li²⁹, Zonghai Li²⁶, An-An Liang³⁰, Jiajun Liao¹⁶, Minghua Liao¹⁶, Yilin Liao²³, Ayut Limphirat⁶⁴, Bo-Chun Lin³⁰, Guey-Lin Lin³⁰, Shengxin Lin¹⁴, Tao Lin⁸, Xianhao Lin²¹, Xingyi Lin²², Jiajie Ling¹⁶, Xin Ling¹⁸, Ivano Lippi⁵², Caimei Liu⁸, Fang Liu⁹, Fengcheng Liu⁹, Haidong Liu²⁹, Haotian Liu²⁶, Hongbang Liu²², Hongjuan Liu¹⁸, Hongtao Liu¹⁶, Hongyang Liu⁸, Jianglai Liu^{23,24}, Jiaxi Liu⁸, Jinchang Liu⁸, Kainan Liu¹⁹, Min Liu¹⁸, Qian Liu¹¹, Runxuan Liu^{45,40}, Shenghui Liu⁸, Shulin Liu⁸, Xiaowei Liu¹⁶, Xiwen Liu²², Xuwei Liu¹⁰, Yankai Liu²⁷, Zhen Liu⁸, Lorenzo Loi⁵⁰, Alexey Lokhov^{60,59}, Paolo Lombardi⁴⁹, Claudio Lombardo⁴⁷, Kai Loo³⁴, Selma Conforti Di Lorenzo³⁶, Haoqi Lu⁸, Junguang Lu⁸, Meishu Lu⁴⁴, Shuxiang Lu²⁹, Xianguo Lu⁶⁶, Bayarto Lubsandorzhiev⁵⁹, Sultim Lubsandorzhiev⁵⁹, Livia Ludhova^{45,43}, Arslan Lukhanov⁵⁹, Fengjiao Luo¹⁸, Guang Luo¹⁶, Jianyi Luo¹⁶, Shu Luo²⁸, Wuming Luo⁸, Xiaojie Luo⁸, Vladimir Lyashuk⁵⁹, Bangzheng Ma²⁰, Bing Ma²⁹, Qiumei Ma⁸, Si Ma⁸, Wing Yan Ma²⁰, Xiaoyan Ma⁸, Xubo Ma⁹, Jihane Maalmi³⁵, Jingyu Mai¹⁶, Marco Malabarba^{45,43}, Yury Malyshkin^{45,43}, Roberto Carlos Mandujano⁶⁷, Fabio Mantovani⁴⁸, Xin Mao⁷, Stefano M. Mari⁵⁶, Agnese Martini⁵⁵, Matthias Mayer⁴⁴, Davit Mayilyan¹, Yue Meng²³, Anselmo Meregaglia³⁶, Lino Miramonti⁴⁹, Marta Colomer Molla², Michele Montuschi⁴⁸, Iwan Morton-Blake²⁴, Massimiliano Nastasi⁵⁰, Dmitry V. Naumov⁵⁸, Elena Naumova⁵⁸, Igor Nemchenok⁵⁸, Elisabeth Neuerburg⁴⁰, Alexey Nikolaev⁶⁰, Feipeng Ning⁸, Zhe Ning⁸, Yujie Niu⁸, Hiroshi Nunokawa⁴, Lothar Oberauer⁴⁴, Juan Pedro Ochoa-Ricoux^{67,5}, Sebastian Olivares⁶, Alexander Olshevskiy⁵⁸, Domizia Orestano⁵⁶, Fausto Ortica⁵⁴, Rainer Othegegraven⁴³, Yifei Pan¹⁶, Alessandro Paoloni⁵⁵, George Parker⁴³, Yatian Pei⁸, Luca Pelicci⁴⁹, Anguo Peng¹⁸, Yu Peng⁸, Zhaoyuan Peng⁸, Elisa Percalli⁴⁹, Willy Perrin³⁷, Frédéric Perrot³⁶, Pierre-Alexandre Petitjean², Fabrizio Petrucci⁵⁶, Oliver Pilarczyk⁴³, Artyom Popov⁶⁰, Pascal Poussot³⁷, Ezio Previtali⁵⁰, Fazhi Qi⁸, Ming Qi²¹, Xiaohui Qi⁸, Sen Qian⁸, Xiaohui Qian⁸, Zhonghua Qin⁸, Shoukang Qiu¹⁸, Manhao Qu²⁹, Zhenning Qu⁸, Gioacchino Ranucci⁴⁹, Thomas Raymond³⁷, Alessandra Re⁴⁹, Abdel Rebii³⁶, Mariia Redchuk⁵², Bin Ren¹⁴, Yuhan Ren⁸, Cristobal Morales Reveco^{45,40,43}, Barbara Ricci⁴⁸, Komkrit Rientong⁶², Mariam Rifai^{45,40,43}, Mathieu Roche³⁶, Narongkiat Rodphai⁸, Fernanda de Faria Rodrigues⁸, Aldo Romani⁵⁴, Bedřich Roskovec³³, Arseniy Rybnikov⁵⁸, Andrey Sadovsky⁵⁸, Paolo Saggese⁴⁹, Deshan Sandanayake³⁷, Anut Sangka⁶³, Ujwal Santhosh^{45,43}, Giuseppe Sava⁴⁷, Utane Sawangwit⁶³, Michaela Schever⁴⁰, Cédric Schwab³⁷, Konstantin Schweizer⁴⁴, Alexandr Selyunin⁵⁸, Andrea Serafini⁵³, Mariangela Settimo³⁹, Junyu Shao⁸, Vladislav Sharov⁵⁸, Hangyu Shi¹⁶, Hexi Shi⁵⁶, Jingyan Shi⁸, Yanan Shi⁸, Vitaly Shutov⁵⁸, Andrey Sidorenkov⁵⁹, Apeksha Singhal^{45,43}, Chiara Sirignano⁵³, Jaruchit Siripak⁶⁴, Monica Sisti⁵⁰, Mikhail Smirnov⁴¹, Oleg Smirnov⁵⁸, Thiago Sogo-Bezerra³⁹, Sergey Sokolov⁵⁸, Julianan Songwadhana⁶⁴, Boonrucksar Soonthornthum⁶³, Albert Sotnikov⁵⁸, Warintorn

Sreethawong⁶⁴, Achim Stahl⁴⁰, Luca Stanco⁵², Konstantin Stankevich⁶⁰, Hans Steiger^{44,43}, Jochen Steinmann⁴⁰, Tobias Sterr⁴⁶, Matthias Raphael Stock⁴⁴, Virginia Strati⁴⁸, Mikhail Strizh⁶⁰, Alexander Studenikin⁶⁰, Aoqi Su²⁹, Jun Su¹⁶, Guangbao Sun²⁶, Mingxia Sun⁸, Xilei Sun⁸, Yongzhao Sun⁸, Zhengyang Sun²⁴, Narumon Suwonjandee⁶², Fedor Šimkovic⁶¹, Christophe De La Taille³⁶, Akira Takenaka²⁴, Xiaohan Tan²⁰, Jian Tang¹⁶, Jingzhe Tang²², Qiang Tang¹⁶, Quan Tang¹⁸, Xiao Tang⁸, Minh Thuan Nguyen Thi³⁰, Yuxin Tian²⁴, Igor Tkachev⁵⁹, Tomas Tmej³³, Marco Danilo Claudio Torri⁴⁹, Andrea Triossi⁵³, Wladyslaw Trzaska³⁴, Yu-Chen Tung⁶⁸, Cristina Tuve⁴⁷, Nikita Ushakov⁵⁹, Carlo Venettacci⁵⁶, Giuseppe Verde⁴⁷, Maxim Vialkov⁶⁰, Benoit Viaud³⁹, Cornelius Moritz Vollbrecht^{45,40}, Vit Vorobel³³, Dmitriy Voronin⁵⁹, Lucia Votano⁵⁵, Caishen Wang¹⁴, Chung-Hsiang Wang³¹, En Wang²⁹, Hanwen Wang⁸, Jiabin Wang²⁰, Jun Wang¹⁶, Li Wang^{29,8}, Meng Wang¹⁸, Meng Wang²⁰, Mingyuan Wang⁸, Qianchuan Wang²⁶, Ruiqiang Wang⁸, Sibo Wang⁸, Tianhong Wang¹⁷, Wei Wang¹⁶, Wenshuai Wang⁸, Xi Wang¹², Yangfu Wang⁸, Yaoguang Wang²⁰, Yi Wang⁸, Yi Wang¹⁰, Yifang Wang⁸, Yuanqing Wang¹⁰, Yuyi Wang¹⁰, Zhe Wang¹⁰, Zheng Wang⁸, Zhimin Wang⁸, Apimook Watcharangkool⁶³, Wei Wei⁸, Wei Wei²⁰, Yadong Wei¹⁴, Yuehuan Wei¹⁶, Zhengbao Wei²², Liangjian Wen⁸, Jun Weng¹⁰, Christopher Wiebusch⁴⁰, Rosmarie Wirth⁴¹, Bi Wu¹⁶, Chengxin Wu¹⁶, Diru Wu⁸, Qun Wu²⁰, Yinhui Wu⁸, Yiyang Wu¹⁰, Zhaoxiang Wu⁸, Zhi Wu⁸, Michael Wurm⁴³, Jacques Wurtz³⁷, Dongmei Xia¹³, Shishen Xian²⁴, Ziqian Xiang²³, Fei Xiao⁸, Pengfei Xiao⁸, Xiang Xiao¹⁶, Wei-Jun Xie³⁰, Xiaochuan Xie²², Yijun Xie⁸, Yuguang Xie⁸, Zhao Xin⁸, Zhizhong Xing⁸, Benda Xu¹⁰, Cheng Xu¹⁸, Donglian Xu^{24,23}, Fanrong Xu¹⁵, Jiayang Xu⁸, Jinghuan Xu²², Meihang Xu⁸, Shiwen Xu⁸, Xunjie Xu⁸, Yin Xu²⁵, Yu Xu¹⁶, Jingqin Xue⁸, Baojun Yan⁸, Qiyu Yan^{11,66}, Taylor Yan⁶⁴, Xiongbo Yan⁸, Yupeng Yan⁶⁴, Changgen Yang⁸, Chengfeng Yang¹⁶, Fengfan Yang⁸, Jie Yang²⁹, Lei Yang¹⁴, Pengfei Yang¹⁶, Xiaoyu Yang⁸, Yifan Yang², Yixiang Yang⁸, Zekun Yang²⁰, Haifeng Yao⁸, Jiaxuan Ye⁸, Mei Ye⁸, Ziping Ye²⁴, Frédéric Yermia³⁹, Jilong Yin⁸, Weiqing Yin⁸, Xiaohao Yin¹⁶, Zhengyun You¹⁶, Boxiang Yu⁸, Chiye Yu¹⁴, Chunxu Yu²⁵, Hongzhao Yu⁸, Peidong Yu⁸, Xianghui Yu²⁵, Zeyuan Yu⁸, Zezhong Yu⁸, Cenxi Yuan¹⁶, Chengzhuo Yuan⁸, Zhaoyang Yuan⁸, Zhenxiong Yuan¹⁰, Noman Zafar⁵⁷, Kirill Zamogilnyi⁶⁰, Jilberto Zamora⁶, Vitalii Zavadskyi⁵⁸, Fanrui Zeng²⁰, Shan Zeng⁸, Tingxuan Zeng⁸, Liang Zhan⁸, Yonghua Zhan¹⁶, Aiqiang Zhang¹⁰, Bin Zhang²⁹, Binting Zhang⁸, Feiyang Zhang²³, Han Zhang⁸, Haosen Zhang⁸, Honghao Zhang¹⁶, Jialiang Zhang²¹, Jiawen Zhang⁸, Jie Zhang⁸, Jingbo Zhang¹⁷, Junwei Zhang²², Lei Zhang²¹, Ping Zhang²³, Qingmin Zhang²⁷, Rongping Zhang⁸, Shiqi Zhang¹⁶, Shuihan Zhang⁸, Siyuan Zhang²², Tao Zhang²³, Xiaomei Zhang⁸, Xin Zhang⁸, Xu Zhang⁸, Xuantong Zhang⁸, Yibing Zhang⁸, Yinhong Zhang⁸, Yiyu Zhang⁸, Yongpeng Zhang⁸, Yu Zhang⁸, Yuanyuan Zhang²⁴, Yumei Zhang¹⁶, Zhenyu Zhang²⁶, Zhijian Zhang¹⁴, Jie Zhao⁸, Runze Zhao⁸, Shujun Zhao²⁹, Tianhao Zhao⁸, Hua Zheng¹⁴, Yangheng Zheng¹¹, Li Zhou⁸, Shun Zhou⁸, Tong Zhou⁸, Xiang Zhou²⁶, Xing Zhou⁸, Jingsen Zhu¹⁶, Kangfu Zhu²⁷, Kejun Zhu⁸, Zhihang Zhu⁸, Bo Zhuang⁸, Honglin Zhuang⁸, Liang Zong¹⁰, and Jiaheng Zou⁸

¹Yerevan Physics Institute, Yerevan, Armenia

²Université Libre de Bruxelles, Brussels, Belgium

³Universidade Estadual de Londrina, Londrina, Brazil

⁴Pontifícia Universidade Católica do Rio de Janeiro, Rio de Janeiro, Brazil

⁵Millennium Institute for SubAtomic Physics at the High-energy Frontier (SAPHIR),
ANID, Chile

⁶Universidad Andres Bello, Fernandez Concha 700, Chile

⁷Beijing Institute of Spacecraft Environment Engineering, Beijing, China

⁸Institute of High Energy Physics, Beijing, China

⁹North China Electric Power University, Beijing, China

¹⁰Tsinghua University, Beijing, China

¹¹University of Chinese Academy of Sciences, Beijing, China

¹²College of Electronic Science and Engineering, National University of Defense
Technology, Changsha, China

¹³Chongqing University, Chongqing, China

¹⁴Dongguan University of Technology, Dongguan, China

¹⁵Jinan University, Guangzhou, China

¹⁶Sun Yat-Sen University, Guangzhou, China

¹⁷Harbin Institute of Technology, Harbin, China

¹⁸University of South China, Hengyang, China

¹⁹Wuyi University, Jiangmen, China

²⁰Shandong University, Jinan, China, and Key Laboratory of Particle Physics and Particle
Irradiation of Ministry of Education, Shandong University, Qingdao, China

²¹Nanjing University, Nanjing, China

²²Guangxi University, Nanning, China

²³School of Physics and Astronomy, Shanghai Jiao Tong University, Shanghai, China

²⁴Tsung-Dao Lee Institute, Shanghai Jiao Tong University, Shanghai, China

²⁵Nankai University, Tianjin, China

²⁶Wuhan University, Wuhan, China

²⁷Xi'an Jiaotong University, Xi'an, China

²⁸Xiamen University, Xiamen, China

²⁹School of Physics and Microelectronics, Zhengzhou University, Zhengzhou, China

³⁰Institute of Physics, National Yang Ming Chiao Tung University, Hsinchu

³¹National United University, Miao-Li

³²Department of Physics, National Taiwan University, Taipei

³³Charles University, Faculty of Mathematics and Physics, Prague, Czech Republic

³⁴University of Jyvaskyla, Department of Physics, Jyvaskyla, Finland

³⁵IJCLab, Université Paris-Saclay, CNRS/IN2P3, 91405 Orsay, France

³⁶Univ. Bordeaux, CNRS, LP2I, UMR 5797, F-33170 Gradignan, F-33170 Gradignan,
France

³⁷IPHC, Université de Strasbourg, CNRS/IN2P3, F-67037 Strasbourg, France

³⁸Aix Marseille Univ, CNRS/IN2P3, CPPM, Marseille, France

³⁹Nantes Université, IMT Atlantique, CNRS/IN2P3, Nantes, France

⁴⁰III. Physikalisches Institut B, RWTH Aachen University, Aachen, Germany

⁴¹Institute of Experimental Physics, University of Hamburg, Hamburg, Germany

⁴²Forschungszentrum Jülich GmbH, Nuclear Physics Institute IKP-2, Jülich, Germany

⁴³Institute of Physics and EC PRISMA⁺, Johannes Gutenberg Universität Mainz, Mainz,
Germany

⁴⁴Technische Universität München, München, Germany

⁴⁵GSI Helmholtzzentrum für Schwerionenforschung GmbH, Planckstr. 1, 64291 Darmstadt (Germany)

⁴⁶Eberhard Karls Universität Tübingen, Physikalisches Institut, Tübingen, Germany

⁴⁷INFN Catania and Dipartimento di Fisica e Astronomia dell'Università di Catania, Catania, Italy

⁴⁸Department of Physics and Earth Science, University of Ferrara and INFN Sezione di Ferrara, Ferrara, Italy

⁴⁹INFN Sezione di Milano and Dipartimento di Fisica dell'Università di Milano, Milano, Italy

⁵⁰INFN Milano Bicocca and University of Milano Bicocca, Milano, Italy

⁵¹INFN Milano Bicocca and Politecnico of Milano, Milano, Italy

⁵²INFN Sezione di Padova, Padova, Italy

⁵³Dipartimento di Fisica e Astronomia dell'Università di Padova and INFN Sezione di Padova, Padova, Italy

⁵⁴INFN Sezione di Perugia and Dipartimento di Chimica, Biologia e Biotecnologie dell'Università di Perugia, Perugia, Italy

⁵⁵Laboratori Nazionali di Frascati dell'INFN, Roma, Italy

⁵⁶Dipartimento di Matematica e Fisica, Università Roma Tre and INFN Sezione Roma Tre, Roma, Italy

⁵⁷Pakistan Institute of Nuclear Science and Technology, Islamabad, Pakistan

⁵⁸Joint Institute for Nuclear Research, Dubna, Russia

⁵⁹Institute for Nuclear Research of the Russian Academy of Sciences, Moscow, Russia

⁶⁰Lomonosov Moscow State University, Moscow, Russia

⁶¹Comenius University Bratislava, Faculty of Mathematics, Physics and Informatics, Bratislava, Slovakia

⁶²High Energy Physics Research Unit, Faculty of Science, Chulalongkorn University, Bangkok, Thailand

⁶³National Astronomical Research Institute of Thailand, Chiang Mai, Thailand

⁶⁴Suranaree University of Technology, Nakhon Ratchasima, Thailand

⁶⁵The University of Liverpool, Department of Physics, Oliver Lodge Laboratory, Oxford Str., Liverpool L69 7ZE, UK, United Kingdom

⁶⁶University of Warwick, University of Warwick, Coventry, CV4 7AL, United Kingdom

⁶⁷Department of Physics and Astronomy, University of California, Irvine, California, USA

⁶⁸Department of Physics, National Kaohsiung Normal University, Kaohsiung

⁶⁹Department of Electro-Optical Engineering, National Taipei University of Technology, Taipei

October 9, 2025

Abstract

Over 25,600 3-inch photomultiplier tubes (PMTs) have been instrumented for the central detector of the Jiangmen Underground Neutrino Observatory. Each PMT is equipped with a high-voltage divider and a frontend cable with waterproof sealing. Groups of sixteen PMTs are connected to the underwater frontend readout electronics via specialized multi-channel waterproof connectors. This paper outlines the design and mass production processes for the high-voltage divider, the cable and connector, as well as the waterproof potting of the PMT bases. The results of the acceptance tests of all the integrated PMTs are also presented.

1 Introduction

The Jiangmen Underground Neutrino Observatory (JUNO) is a particle physics experiment currently under construction, aiming for neutrino studies and exotic searches [1, 2, 3]. The central detector [4] is made of a 20 kiloton liquid scintillator target surrounded by 17,612 20-inch [5] and 25,600 3-inch photomultiplier tubes (PMTs) [6], all of which are submerged in water at a depth of up to 43.5 m along with their frontend electronics.

By virtue of their operation in single photon-counting mode at reactor antineutrino energies, the 3-inch PMT system provides a linear reference for calibrating any instrumental non-linearities in the charge response of the 20-inch PMTs [7, 8]. The 3-inch PMTs also improve the energy resolution [9], enhance event reconstruction [10], aid cosmic muon tracking [11], and support several physics measurements, including proton decay searches [12], and the measurement of the solar oscillation parameters θ_{12} and Δm_{21}^2 , for which they provide a semi-independent determination [13].

The system is divided into 200 readout units of 128 PMTs each. A diagram of one such unit is shown in Fig. 1. Each PMT is equipped with a high voltage (HV) divider and a coaxial cable that can be 5 m or 10 m in length and that transmits both the HV and the signal. The PMT, HV divider, and one end of the cable are soldered and waterproofed. The other ends of sixteen cables are connected to a multichannel connector, each consisting of a plug and receptacle pair. These connectors are linked to an underwater stainless steel box (UWB), housing the 128-channel frontend power supply and readout electronics. This paper provides details on the instrumentation of the 3-inch PMTs, encompassing the design and production of the HV divider, cable, and connector, as well as the waterproof potting and the acceptance tests. The production and characterization of 26,000 (including 400 spares) 3-inch PMTs was reported in Ref. [6]. The electronics design was outlined in Ref. [3, 14, 15].

The rest of this paper is structured as follows. In Sec. 2 and 3, the research and development, as well as the manufacturing process of the HV divider, cable, and connector, are presented. The waterproof potting is detailed in Sec. 4. Section 5 covers the acceptance tests following potting. Section 6 provides a summary. Unless otherwise specified, all references to PMTs in the subsequent sections pertain to the 3-inch PMTs.

^{*}xujl@ihep.ac.cn

[†]hem@ihep.ac.cn

[‡]cedric.cerna@in2p3.fr

[§]huangyb@gxu.edu.cn

[¶]Now at Emirates Nuclear Technology Center (ENTC), Khalifa University, Abu Dhabi, United Arab Emirates.

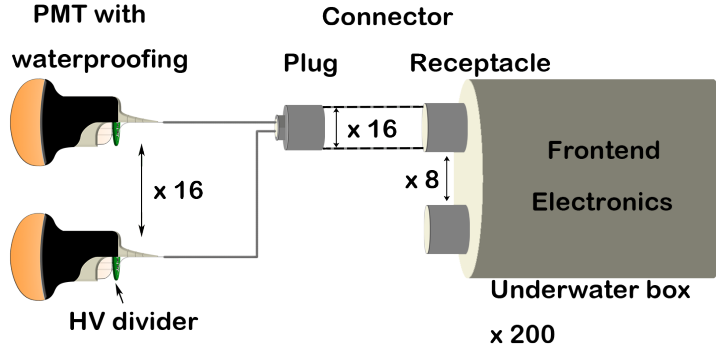


Figure 1: Diagram of a readout unit, consisting of 128 3-inch PMTs linked to underwater electronics through eight 16-channel connectors.

2 HV Divider

The HV divider follows a positive HV scheme. The HV ratio for the 11 series of dynodes is optimized for collection efficiency and timing measurements [16, 17, 18]. The resistor ratio for the first three dynodes is 3:2:1, and the other resistors are equal in value to the third one, 15 M Ω (Fig. 2 (a)). The total resistance of 210 M Ω and a working HV generally less than 1,300 V result in a gain of approximately 3×10^6 and a direct current (DC) less than 6.5 μ A. In consideration of safety and reliability requirements, the HV divider components include wire resistors, as depicted in Fig. 2 (b), due to superior voltage and thermal tolerance. The main challenge lies in the dense packing of components on the small PCB, which is designed to be soldered directly to the PMT pins and is constrained to have a similar size as the 48 mm diameter of the PMT glass bulb neck. Considering the re-evaluated requirements of the 3-inch PMT system for JUNO, the reliability requirement for the HV divider was slightly relaxed compared to the 20-inch PMT HV divider [5], allowing for the use of surface-mounted components. The final design is illustrated in Fig. 2 (c), where resistors of type 1206 with a maximum of 200 V and a 0.25 W power rating are selected, along with ceramic DC capacitors. The failure rate of the HV divider, as determined from reliability of individual components, is less than 0.05% per year.

The HV divider is designed to achieve a maximum working HV of 2,000 V using a single layer of standard FR-4 [19] PCB material with a thickness of 1.2 mm and a diameter of 47 mm, in compliance with the radioactivity requirements of JUNO [20]. The PCB design ensures a clearance exceeding 1.6 kV/mm. Testing was performed on a few random samples of the final products, where HV dividers were subjected to several weeks of operation up to 2,400 V with satisfactory performance, and a maximum of 3,000 V was applied for a short period without failure. The flasher rate of the HV divider was verified to be less than 1 mHz, as detailed in Ref. [21]. To mitigate potential risks of flasher occurrences during production and long-term operation, black polyurethane was used to cover the divider PCB after it has been soldered to the PMT pins, as will be discussed in Sec. 4. A temperature cycling test was successfully conducted on 20 samples for 10 cycles without any failures, subjected to temperatures ranging from 5°C to 55°C for three hours per cycle. The signal quality coupled with the 3-inch PMT was further assessed in Ref. [22, 23], with additional results to be discussed in the following sections.

Viking [24] surface bounding resistors of type 1206 and Murata [25] ceramic capacitors were chosen for the design. In adherence to the JUNO divider PCB procedure [21], mass production was executed after a successful small batch production of 100 pieces, all of which passed testing. All PCBs were soldered at the factory following cleaning at the designated soldering points. Subsequently, a visual inspection of the soldering points was performed. After another round of cleaning, each PCB underwent a 30-second maximum

HV test at 2,000V before being soldered to the PMT and the cable. In total, 26,500 divider boards were produced which includes 900 spares. Acceptance tests were conducted during integrating with PMTs, as discussed in Sec. 4.2.

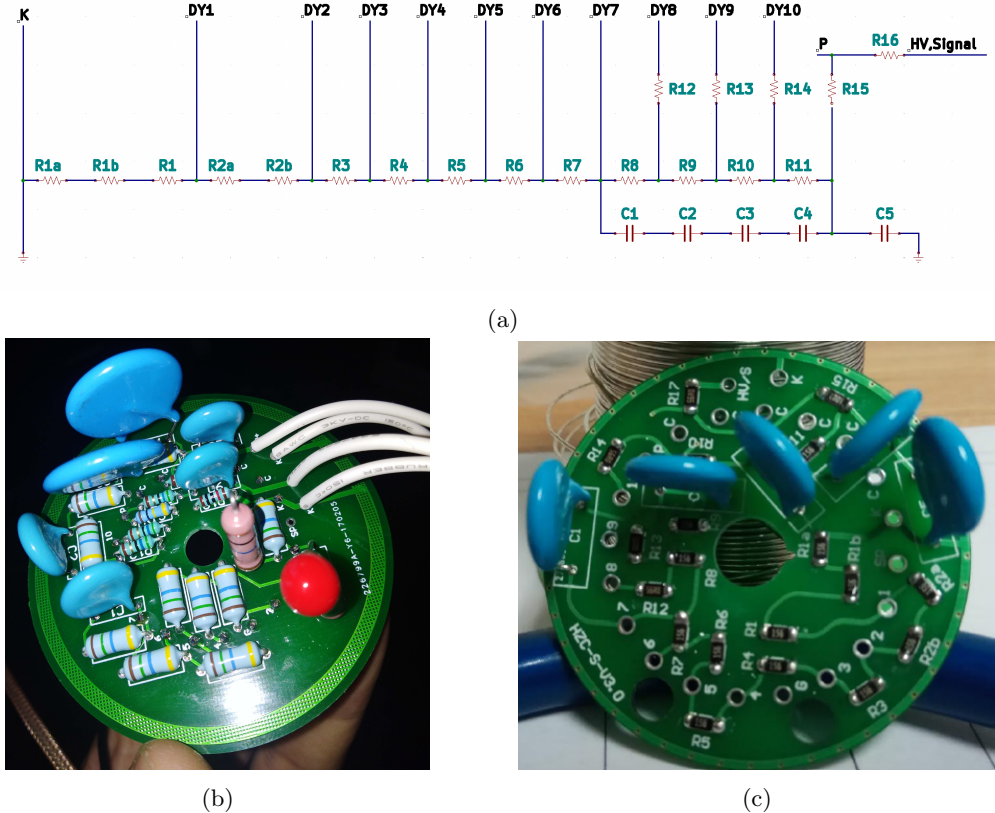


Figure 2: (a) Schematic design of the 3-inch PMT HV divider. R1 to R11 are divider resistors, each with a resistance of $15\text{ M}\Omega$. K denotes the cathode, DY1 to DY10 represent the ten dynode stages, and P indicates the anode. C1 to C4 are decoupling capacitors, each with a capacitance of 10 nF , used to maintain the signal linearity. R12 to R14 are damping resistors, each with a resistance of $56\text{ }\Omega$, to prevent signal ringing. R15 ($100\text{ k}\Omega$) and C5 (4.7 nF) together form a low-pass filter. R16 is a matched resistor with a resistance of $56\text{ }\Omega$. (b) Initial version of the divider with wire resistors. (c) Final version of the divider with surface-mounted resistors.

3 Cable and Connector

3.1 Design

To reduce costs and facilitate the installation of the JUNO detector, a novel 16-channel waterproof connector and cable was designed in collaboration with AXON' company [26]. The connector's schematic design is shown in Fig. 3 and consists of two parts: a plug that is attached to 16 PMTs through frontend cables, and a receptacle that is mounted on the UWB. Waterproof sealing between the 16 cables is achieved through

injection molding in the plug and the application of adhesive in the receptacle. A double-sealing design ensures tightness when the plug is connected to the receptacle.

The receptacle is approximately 25 cm in length and contains 16 specialized micro coaxial connector plug pins. These connector plugs are mounted on a special thermoplastic shell, which is subsequently inserted into the stainless steel shell of the receptacle. This design ensures that the cable grounding remains isolated from the receptacle shell, thus meeting JUNO's requirement of signal grounding to be separated from grounding of the JUNO mechanical structure. The end of the receptacle shell is sealed with epoxy, providing the receptacle with independent waterproof capability, regardless of whether the plug is connected. Eight receptacles are mounted on the lid of the UWB. Even if one plug fails, the receptacle is designed to prevent water from entering the UWB, thereby protecting the internal electronics.

A custom-made RG178 coaxial cable with a $50\ \Omega$ impedance was also developed. The outer layer of the cable is made of High-Density Polyethylene (HDPE) with a diameter of 2.1 mm, designed to prevent fluorescence and ensure long-term reliability in ultra-pure water environment. As an additional safeguard, a water-blocking powder, developed by AXON' company, was incorporated into the grounding layer. If the cable jacket is compromised, water would penetrate this layer, activating this barrier and preventing further water ingress. A water pressure test demonstrated that after one hour under 5 bar pressure, water infiltration was restricted to only 5 cm.

During the commissioning phase of the JUNO detector, a few weeks after the start of water filling, a significant number of channels experienced HV breakdown. This issue was traced to air diffusing from the connectors toward the ultra-pure degassed water, resulting in a pressure drop within the connector assembly. To address this problem, a continuous flow of nitrogen gas was introduced into the water circulation system, effectively resolving the issue. The 3-inch PMT system was integrated into detector operation following the completion of liquid scintillator filling. The operating power of each PMT group is being continuously monitored and has remained stable. Further details and comprehensive analysis of this incident will be provided in an upcoming publication.

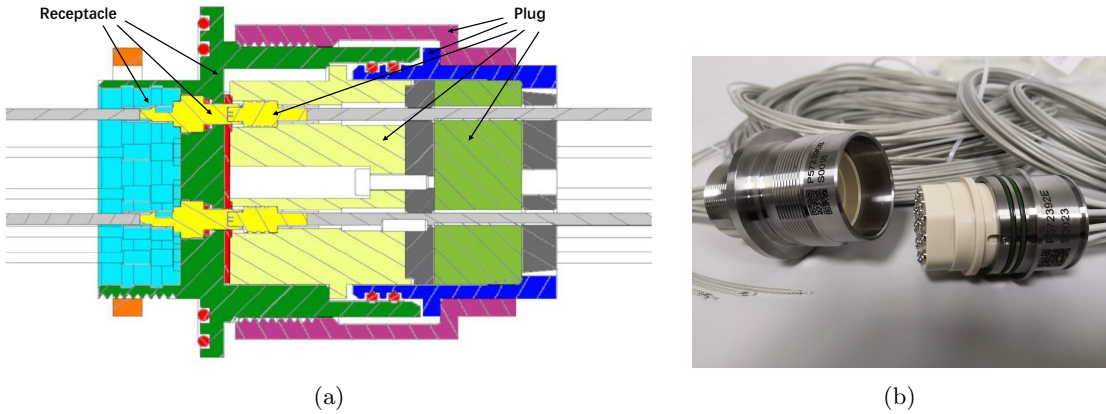


Figure 3: (a) Schematic design of the 16-channel connector consisting of a plug (left part) and a receptacle (right part). The red dots and lines indicate water-resistant O-rings or gaskets. Due to intellectual property rights, further details cannot be disclosed. (b) A picture of a connector set with cables.

3.2 Signal Performances

The quality of the PMT signal was examined using a prototype of the connector and cables, as detailed in Ref. [23]. Typical signals for the single photoelectron (SPE) with a gain of 3×10^6 are displayed in Fig. 4 (a).

Small reflections following the main signal, attributed to a slight impedance mismatch not to the connector but in the hand-made HV-signal splitter, were observed. This issue was resolved in the final version of the splitter as reported in Ref. [15]. To compensate for the loss of PMT gain due to cable attenuation, an additional 23 V or 45 V voltage was applied for 5 m or 10 m cables, respectively. The observed amplitude, rise time, fall time, and Full Width at Half Maximum are listed in Tab. 1.

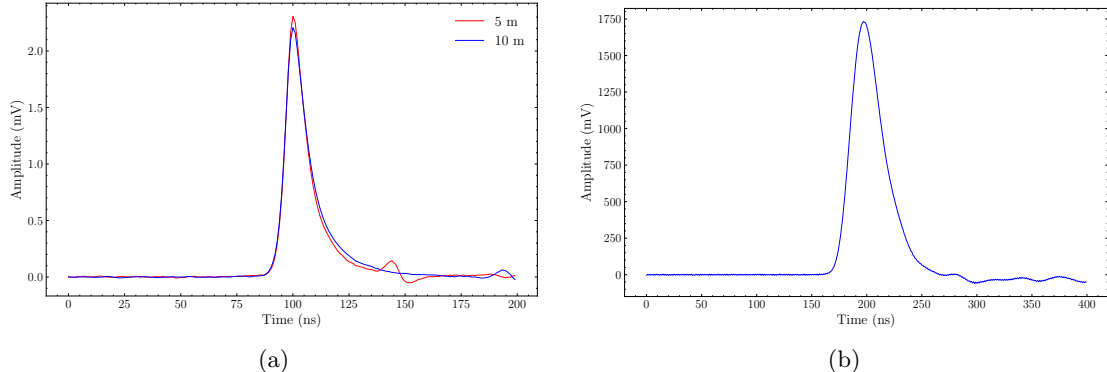


Figure 4: (a) An average PMT signal for the single photoelectron using a 5 m (red) or 10 m (blue) cable. The reflection, resulting from a slight impedance mismatch in the prototype HV splitter, was addressed and resolved in the final version of the splitter [15]. (b) The average PMT signal with a large light intensity of approximately 4,000 photoelectrons.

Table 1: Measured features of PMT SPE signals with cable length 5 m and 10 m at a gain of 3×10^6 . Errors are statistical only.

| | Gain 3×10^6 | 5 m | 10 m |
|----------------|----------------------|------------------|------|
| Amplitude (mV) | 2.25 ± 0.08 | 2.16 ± 0.08 | |
| Rise time (ns) | 4.29 ± 0.12 | 4.57 ± 0.12 | |
| Fall time (ns) | 15.65 ± 0.16 | 18.68 ± 0.14 | |
| FWHM (ns) | 11.76 ± 0.12 | 12.98 ± 0.12 | |

The measured PMT charge is not proportional to the number of incident photoelectrons due to both internal factors, such as the space charge effect, and external factors, such as the divider current [27]. Fractional loss of charge, known as nonlinearity, was observed in the JUNO 3-inch PMTs and reported in Ref. [28]. The nonlinearity remains under 5% below 750 PEs but increases significantly above that due to the low divider current (less than $6.5 \mu\text{A}$). An average signal of approximately 4,000 incident PEs obtained with high-intensity LED lights is shown in Fig. 4 (b). The integrated charge corresponds to 2,342 PEs when comparing with the single PE signal in Fig. 4 (a), which represents about 40% charge nonlinearity. However, this nonlinearity is not an issue for JUNO, because the 3-inch PMTs operate in SPE regime for most physics cases.

The crosstalk for a complete assembly of cables, plugs and receptacles was assessed using an adapted network analyzer (Agilent E5062A) [29]. Considering two adjacent channels as the extreme case, in the frequency range of interest from 100 MHz to 350 MHz, an S-parameter analysis verified that the analog charge crosstalk between different channels is less than 0.3%.

3.3 Long Term Validation

The JUNO 3-inch PMT system was designed to achieve a channel failure rate lower than 10% over a 6-year period, equally distributed among the PMTs and their readout electronics. This translates into an estimated Mean Time Between Failure (MTBF) exceeding 120 years, or equivalently, a Failure In Time (FIT) value below 1,000. This requirement applies directly to the cables and connectors that interface with the photomultipliers. Estimating such a low failure rate is challenging when dealing with a limited number of components over a short testing period. For instance, evaluating the reliability of two underwater connector plug and receptacle systems would necessitate a 40-year assessment. In ultra-pure water, the primary cause of long-term failure is chemical degradation, which compromises the protective barriers against water ingress such as cable jackets and connector gaskets. The test duration can be accelerated by subjecting the system to increased temperatures in a controlled setting. Compared to JUNO's operational water temperature of 21°C, raising the temperature by an additional 10°C can expedite the testing process by a factor of approximately 2.5. Thus, a test conducted at 60°C for 12 months simulates the effect of 40 years of ageing at the normal operational temperature of 21°C.

To conduct the test, two pressurized water tanks were developed and equipped - one located in France and the other in Chile. These tanks allowed for the adjustment of water temperature and pressure from 1 to 10 bars to simulate various depths in JUNO. In the test conducted in France, four underwater connectors with 10-meter long cables were mounted on their receptacles. An electric potential ranging from 0 to 2 kV was applied to each cable, with the leakage current monitored at the micro-ampere level, allowing for the detection of any minor water leaks on the cable jacket or at the connector level. In Chile's test, five receptacles and three mechanical models were mounted on the UWB to evaluate long-term water leakage aging under conditions involving heat and pressure.

After the facilities were qualified, the following test campaigns were carried out:

- A first period of 12 months between December 2020 and November 2021, with overpressure cycling between 5 to 10 bars and temperature varying between 55°C and 62°C in France;
- A second period of 4 months between December 2021 and March 2022, with overpressure between 1 to 2 bars, mimicking shallow water, and a temperature varying between 15°C and 20°C in France.
- Five receptacles with water temperature 88.7°C and pressure from 4 to 9 bars, average 7.75 bars were tested in 2021 in Chile.

During the two testing phases conducted in France, spanning over 11,000 hours, no leaking current was observed, and both the cable and connector functioned perfectly, achieving the required reliability with a FIT value smaller than 500. During the destructive test conducted in Chile, five receptacles were aged to the equivalent of over 120 years and exhibited no leaks, yielding a FIT value of 350.

3.4 Production and Quality Inspection in Axon¹

Approximately 200 km of cables were produced and thoroughly tested, with 100% of the insulation verified through a 3,000 V spark test. After the cabling and overmolding processes were finalized, each plug was tested with 1.8 kV of HV for 70 seconds to confirm functionality. Subsequently, the plugs were equipped with stainless steel accessories that matched those of the receptacle. The sealing was achieved using a double sealing design.

The sealed cables and plugs were placed into a stainless steel tank filled with ultrapure water, as shown in Fig. 5. Humidity test paper was also added. The tank was closed, and the water pressure was raised

to 0.75 MPa, maintained for two hours. Once removed from the water tank and dried, the water sealing was verified through visual inspection of the humidity test paper and a subsequent HV test. All cables and connectors underwent testing. Those passing the tests were then used to create the required 10 m and 5 m segments.



Figure 5: Leak test in a high-pressure water tank at AXON'. The dual-end plugs were sealed with fake receptacles and directly put into water. The receptacles were mounted on the lid of the tank.

For each batch, the first and last receptacles were mounted on the lid of the water tank with the 16 pins to be submerged in water (Fig. 5). If these two receptacles passed the test, the remaining receptacles from the batch proceeded to the next step, which involved attaching the micro coaxial connector to the other end of the cable that connects to the electronics in the UWB. In the case of failure, a more thorough inspection and additional destructive pressure testing were conducted on the batch in question. Finally, the receptacle underwent the standard HV test at 1.8 kV for 70 seconds.

In total, 825 plugs of 10 meters in length and 825 plugs of 5 meters in length, along with 1,650 receptacles (including 50 spares), were produced and delivered to JUNO.

3.5 Acceptance Tests by JUNO

A warehouse designated for the JUNO 20-inch PMT mass testing [5] was also used for the storage and acceptance tests of the 3-inch PMT cables and connectors. The initial step involved visual inspections to detect any visible damage or defects, with particular attention paid to scratches on the sealing surfaces of the connectors. Electrical tests followed, assessing the resistance and electrical conduction of the core wire and the braid grounding wire, as well as verifying the channel sequence from 1 to 16. Additionally, HV testing (1.6 kV, > 5 minutes) was carried out to determine the cables' ability to withstand voltage stress and confirm their safe operation under normal conditions. Since only two receptacles from each batch underwent destructive tests underwater at Axon', a supplementary leak test with SF₆ gas was conducted for

10% of the receptacles. Each selected sample was sealed with a fake plug using an axial O-ring, evacuated to below 50 Pa, maintained for one minute, and then filled with SF₆ gas at a pressure about 25% higher than standard atmospheric pressure. An SF₆ detector was used outside the receptacle to detect any leaked gas with a sensitivity of 10⁻⁸ Pa·m³/s [30]. No leakage was detected in any of the tested receptacles.

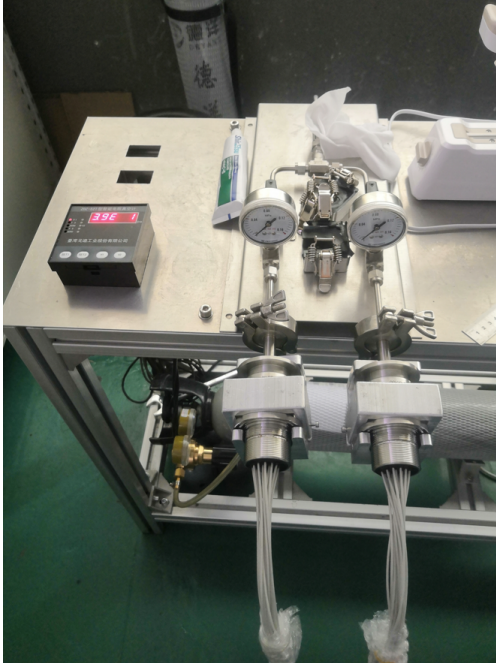


Figure 6: An SF₆-based leakage test facility during inspection. Two receptacles undergo evacuation and are subsequently filled with SF₆ gas to perform the leakage test.

4 Integration and Waterproof Potting

4.1 PMT Grouping

The 26,000 qualified and delivered bare PMTs [6] were assembled into groups of 16 according to their working HV at a gain of 3×10^6 . Additionally, to minimize the risk of PMT implosion underwater, these PMTs were grouped according to their weights and installed at similar depths in the JUNO detector.

Grouping by HV

The operating HV required to achieve a gain of 3×10^6 for each PMT was determined by the manufacturer, with the distribution shown in Fig. 7. The voltage ranges from 900 V to 1,300 V. PMTs with working voltage outside of this range were excluded from mass production [6]. The voltages were categorized into 16 groups, each spanning 25 V, with a maximum gain difference of 15% to 20% within each group.

Grouping by weight

PMTs are made of quartz glass with an average thickness between 1 mm and 2 mm. During long-term operation in water at a 42 m depth, buckling failure may happen due to large external pressure. For an ideal spherical shell, the classical critical buckling pressure p_b can be expressed as [31]

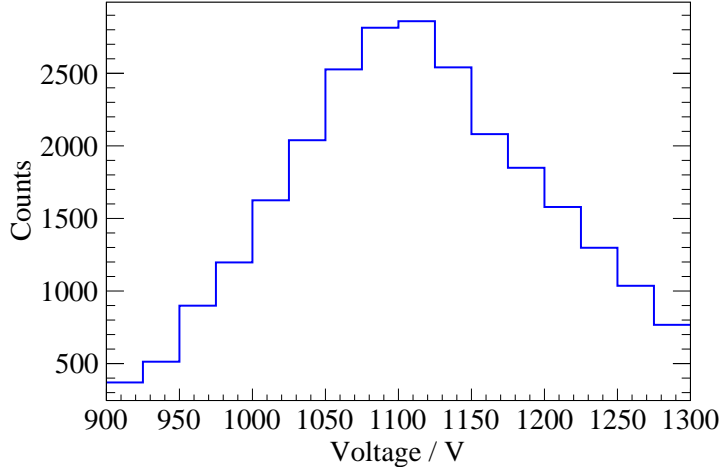


Figure 7: Distribution of working voltage at 3×10^6 gain of PMTs.

$$p_b = \frac{2E}{\sqrt{3(1-\nu^2)}} \frac{t^2}{r^2}, \quad (1)$$

where ν is the Poisson's ratio, E is the tensile modulus, and r and t are the radius and thickness of the glass shell, respectively. Since ν and E are constants for the PMT glass shell, and the shape (r) is almost fixed, the critical pressure is sensitive to the thickness of the glass and thus to the weight.

A dedicated study was done to find the dependence of the critical pressure on the weight of the PMT. Ten PMTs were randomly selected from an early production batch and their weights were measured. All pins on the bottom of the PMT were sealed with polyurethane and each PMT was individually put into a water tank. The water pressure was increased with a water pump at a speed of about 0.5 MPa/min. When the PMT glass imploded, the water pressure was recorded.

Critical pressures at different PMT weights are shown in the bottom panel of Fig. 8. A positive correlation can be seen. However, there is a large spread from 1.5 MPa to 2.5 MPa in the 110 g to 115 g range, which can be attributed to variations in the glass shell thickness, as implosions typically initiate at points with the smallest thickness or highest stress. A parabolic function (red dashed curve) is used to fit the critical pressure distribution, but with large fluctuation due to the special shape (not ideal spherical) and non-uniform thickness of the glass shell, as well as the weight of electric components inside the shell.

The weights of all 26,000 PMTs were measured and the resulting distribution is shown in the top panel of Fig. 8. They were categorized into three classes based on their weights and installed at maximum water depths of 10 m, 25 m, and 42 m, respectively, as detailed in Tab. 2. The critical pressure for each class is approximately five times greater than the expected water pressure. Only 3.8% of PMTs fall into class W1 and were installed near the top of the JUNO detector at less than 10 m depth. About 40.5% PMTs, belonging to class W2, were installed on the upper hemisphere of the JUNO detector at depths smaller than 25 m. The remaining PMTs, comprising more than half of the total, belong to class W3 and were installed mostly on the lower hemisphere.

In total, 48 groups were formed, comprising three weight-based groups and 16 HV-based groups. During the potting process, PMTs were selected from groups that were as homogeneous as possible. The installation depth was determined based on the lightest PMT in each assembly.

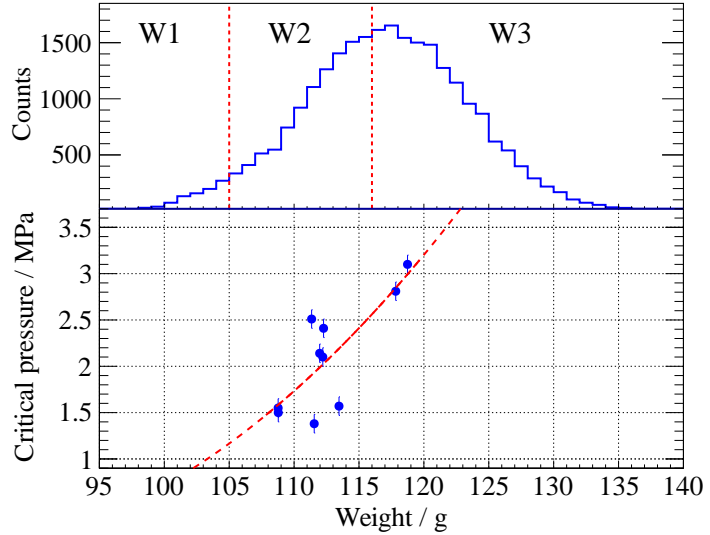


Figure 8: The top panel shows the measured weight distribution for all 26,000 PMTs. W1, W2, and W3 represent three groups of PMTs according to their weights. The blue points in the bottom panel are the measured critical pressures underwater as a function of the PMT weight. The red dashed line is the best fit parabola.

Table 2: Classification of PMTs by weight.

| Class | Fraction | Weight | Installation depth | Water pressure in the leakage test |
|-------|----------|--------------|--------------------|------------------------------------|
| W1 | 3.8% | [90, 105] g | <10 m | 0.20 MPa |
| W2 | 40.5% | [105, 116] g | <25 m | 0.40 MPa |
| W3 | 55.7% | [116, 150] g | <42 m | 0.65 MPa |

4.2 Waterproof PMT Potting

The schematic design of the waterproof PMT potting is illustrated in Fig. 9. The PMT pins, the HV divider, and the cable are soldered and enclosed in an ABS plastic shell. This shell is filled with polyurethane to protect the electrical components from water and to block any light that might be emitted spontaneously by electrical discharges. The seal between the shell and the PMT glass is achieved using butyl tape, which is encompassed by a shrinkable tube and finished with low-pressure injection molding at the end.

As a final verification of the waterproof potting design, 50 samples were produced using PMT glass bulbs or discarded PMTs along with HV dividers and short cables. The cable ends were sealed with epoxy, and all samples were submerged in a water tank in four separate batches, subjected to a pressure of 0.6 MPa for a minimum of 7 days. A potential difference of 2,000 V was applied through the cable ends, and currents were measured both before and after the high-pressure water test. The observed differences ranged from -40% to 70%, which can be attributed to variations in PMT exposure to light. If water had penetrated into the PMT pins or the divider, the current would have increased significantly, by at least an order of magnitude.

The primary steps involved in the potting are illustrated in Fig. 10 (a). An injection-molded ABS plastic shell was designed to provide mechanical support. Initially, the cable was threaded through a bottom entrance with a diameter of 2.2 mm, ensuring 28 cm of the cable remained inside the shell. Following this, epoxy was injected from the top to offer a bonding length greater than 8 cm, serving as the inner seal. The epoxy used is specialized for HDPE, featuring a bonding strength of 1.6 MPa. The sealing was further

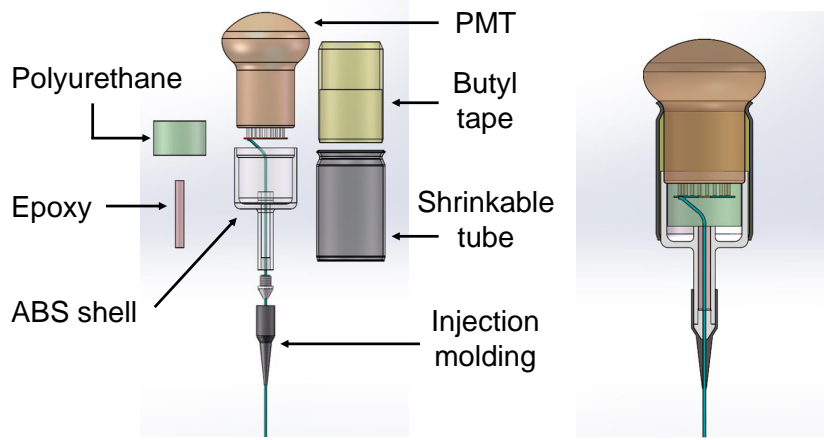


Figure 9: Schematic design of waterproof PMT potting.

reinforced outside the shell's tail through low-pressure injection molding with a polyamide and polyolefin mixture, also customized for HDPE.

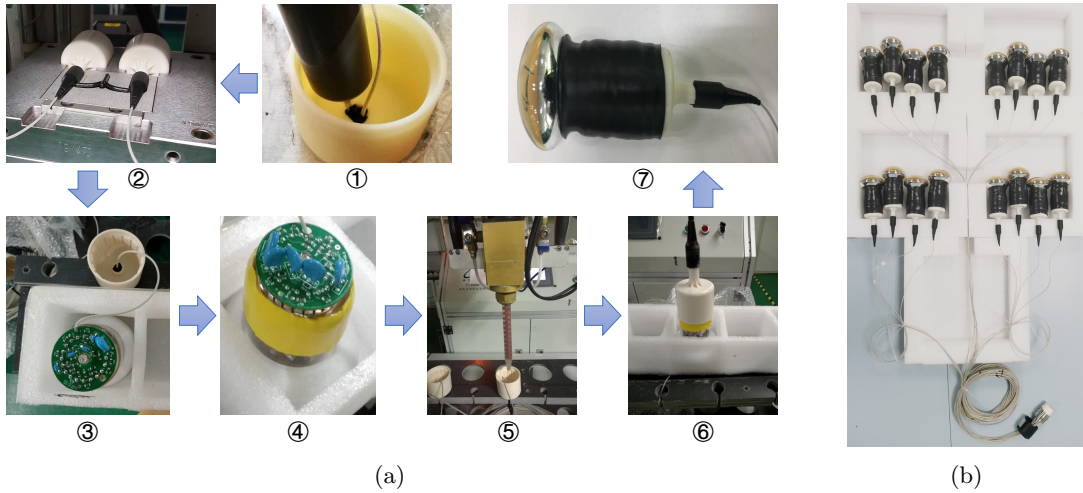


Figure 10: (a) Major steps of waterproof PMT potting: 1, cable sealing with epoxy; 2, cable sealing with injection molding; 3, soldering HV divider on the bare PMT; 4, assembly of butyl tape around the PMT; 5, filling polyurethane; 6, inverting the PMT; 7, covering the shrinkable tube. The PMT signals were verified after step 3 and step 7 with HV. (b) A group of 16 PMTs with cables and the connector after waterproof potting.

Subsequently, the PMT was mounted and soldered onto the HV divider along with the cable. A set of 16 PMTs with plugs were then transferred to a dark box, where each channel was connected to a splitter box to separate the HV and the signal. A nominal HV was applied to each channel, and the current was monitored using an ammeter. Utilizing low-intensity LED lights inside the dark box, PMT signals, predominantly SPEs, were captured by an oscilloscope. The amplitude was required to be within $\pm 50\%$ of the average. If a significant deviation was detected, the PMT was replaced, and the process was repeated for a new PMT.

A fixed volume of a two-part polyurethane adhesive was mixed and filled into the potting shell. The adhesive did not completely fill the potting shell, leaving a few milliliters of air to allow for sealant expansion due to temperature changes. The PMT glass was encircled by a 5 cm wide layer of butyl tape near the bottom of the PMT and positioned in the shell, where a pedestal provided mechanical support. This butyl tape filled the gap between the PMT glass and the shell. The PMT with the potting shell was inverted to ensure complete coverage of all electrical components by the polyurethane, and it was left for 24 hours to allow the polyurethane to cure. A second layer of butyl tape was then added outside the shell as an outer seal, with a 2 cm overlap on the first layer. Finally, a plastic shrinkable tube was added to protect the layers of butyl tape. The fully potted PMTs were tested again to verify signal quality. A picture of an integrated group of 16 PMTs is shown in Fig. 10 (b).

4.3 Leakage Test

A large steel water tank was utilized to conduct a sampling test on potted PMTs to verify water leakage, as depicted in Fig. 11. A group of 16 PMTs was secured on a rack, with the plug sealed using two O-rings within a customized receptacle. Nine groups of PMTs of identical weight classification were simultaneously placed in the tank. The water pressure was elevated according to the weight specifications listed in Table 2 and maintained for 48 hours. Subsequently, the PMTs were removed from the tank, rinsed with pure water, and dried in an oven at 55°C. The PMTs were then subjected to HV testing, and signals were measured for the third time in the dark box.

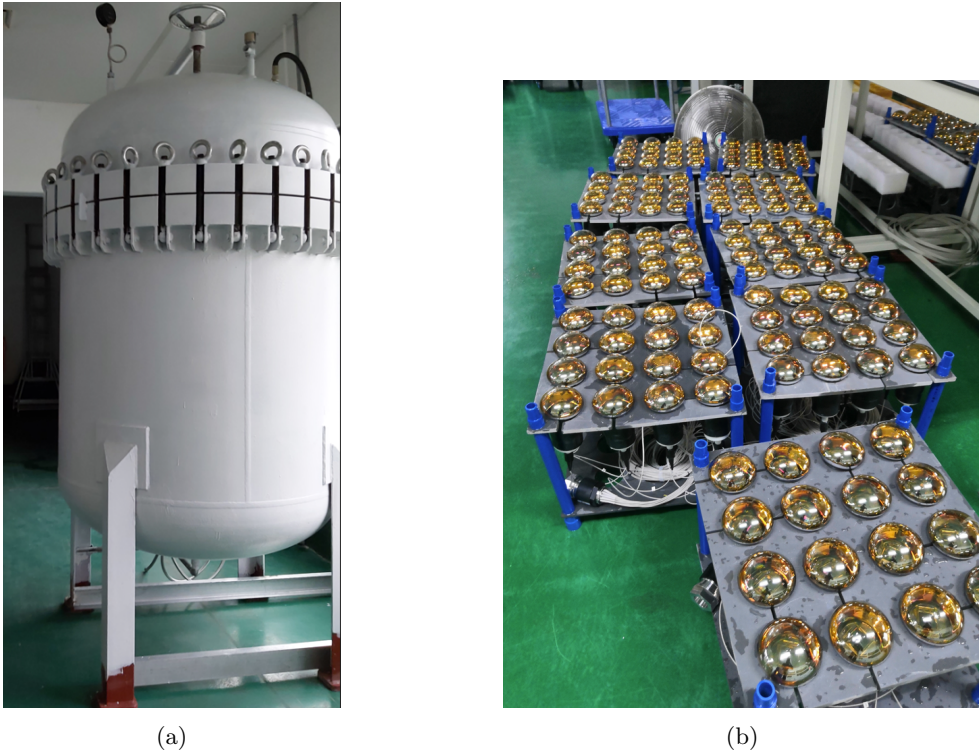


Figure 11: (a) Water tank used for the PMT potting leak testing. (b) Nine groups of PMTs taken out of the tank after 48 hours. Each group of 16 PMTs was fixed on a plastic rack.

A total of 217 groups of PMTs, constituting approximately 13% of the entire collection, were randomly selected from all three weight classes and subjected to underwater testing.

No potting leaks were detected in any of the groups. Nevertheless, four PMT glasses fractured during the water pressure test. Of these, two belonged to weight class W1, and the other two to weight class W2. The failure rate was approximately 0.1%. These PMTs were subsequently replaced.

5 Acceptance Test of Potted PMTs

After potting, all PMTs underwent another round of testing to ensure their reliability and performance prior to being delivered to the JUNO site. This section provides details of the acceptance tests conducted.

5.1 Test Station

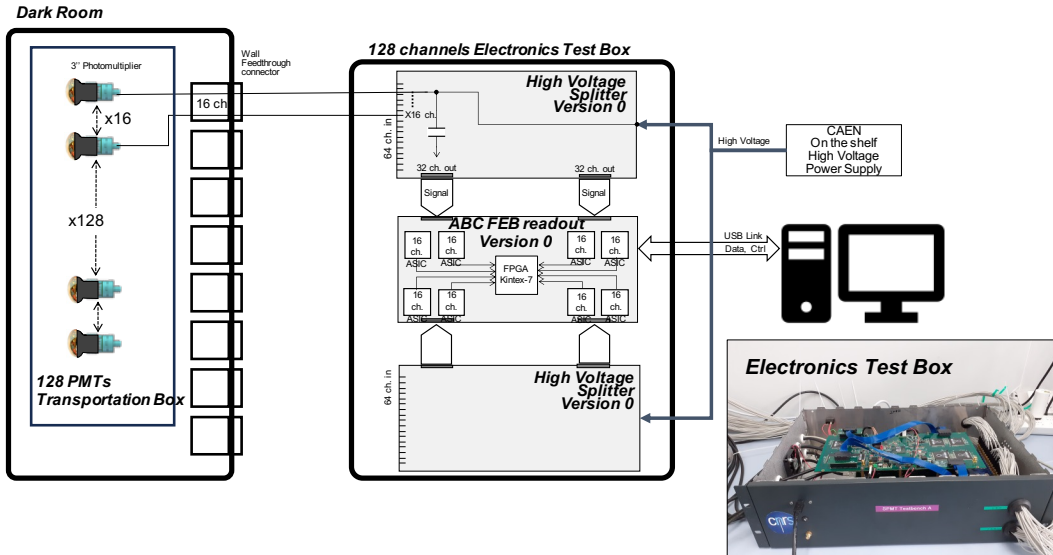


Figure 12: Schematics of a 128-channel PMT acceptance test station and an image of a 128-channel electronics test box.

To ensure efficiency and speed during testing, a test station consisting of two test benches was constructed at Guangxi University (GXU). Each test bench can simultaneously handle eight groups of PMTs. The acceptance test setup included a dark room where the PMT transportation and storage boxes can be placed. Without removing the PMTs from their boxes, they can be connected via feedthrough wall connectors to a 128-channel electronic test box. Figure 12 provides a schematic view of the complete acceptance test system and a photo of the electronics box. This test box is an early simplified prototype of the electronics system. It comprised a 128-channel front-end readout board called the ABC (ASIC Battery Card), connected to the photomultipliers through two 64-channel splitter boards [15]. The prototype ABC board was equipped with 8 CATIROC ASIC chips [14]. Each prototype splitter board was designed to receive four HV inputs from a commercial HV power supply while still handling 64 channels. The firmware and software were customized for the acceptance test scenarios.

5.2 Acceptance Criteria

The characterization of bare PMTs was conducted at the factory of Hainan Zhanchuang Photonics Technology Co., Ltd (HZC) [32], as noted in Ref. [6]. The primary objective of the acceptance tests was to verify the functionality of each PMT following waterproof potting. Consequently, three main performance parameters were established as acceptance criteria, based on experimental requirements detailed in Table 3. The consistency of the working HV is a crucial parameter because groups of potted PMTs share the same HV. When the average gain for each group of PMTs is 3×10^6 , the gain of each PMT should range between 2×10^6 and 5×10^6 . The SPE resolution of each PMT must be less than 45%, and the dark count rate (DCR) must be lower than 3 kHz.

Table 3: Acceptance test criteria.

| Parameters | Requirements |
|----------------|----------------------|
| Gain | $[2, 5] \times 10^6$ |
| SPE resolution | < 45% |
| Dark rate | < 3 kHz |

5.3 HV Calibration Testing

The working HV for the potted PMTs is higher than that of the bare tubes. This is because, firstly, the HV for potted PMT is supplied through an HV splitter. Each channel's $20 \text{ M}\Omega$ current-limiting resistor reduces the HV available to the tube by approximately 10%. Secondly, as discussed in Sec. 3.2, any attenuation in the long cable is compensated by applying a slightly higher HV. At the start of the acceptance test, the working HV for achieving a gain of 3×10^6 (designated as GXU HV) was determined by systematically scanning various HV levels for small batches of PMTs. This value was then compared with the working HV determined from bare tube testing by the PMT manufacturer HZC (referred to HZC HV, with each increment of 25 V represents a distinct HV level). This comparison resulted in a linear relationship, as depicted in Fig. 13.

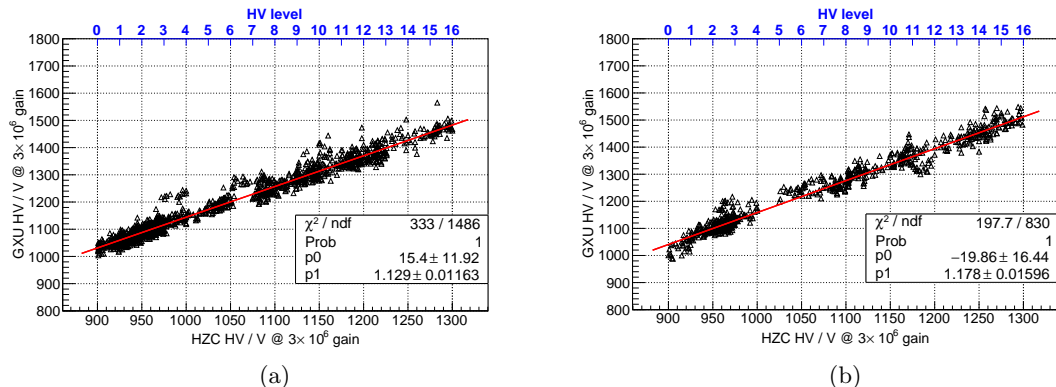


Figure 13: Correlations between GXU and HZC HV measurements. The red line is the result of a simple linear fit to the data. (a) The cable length is 5 meters. (b) The cable length is 10 meters.

Utilizing this correlation, the working HV for each group of PMTs can be easily derived from their HZC HV values during acceptance testing. Subsequent tests confirmed the effectiveness of this procedure, as only

a small number of PMT groups required further adjustments to their working HV during testing. These instances were often due to the challenge of assembling 16 PMTs with identical HV levels into a complete set during waterproof potting, resulting in PMTs with significantly different HV levels being included in the same group. Once all PMTs are installed in the JUNO detector, the scanning will be conducted again for every group to determine the precise working HV.

5.4 Test Results

As stated in Sec. 5.1, for the efficient batch acceptance testing of 26,000 PMTs, we employed two test benches capable of simultaneously measuring 128 PMTs per test setup. The PMTs were placed inside a storage box and shielded in a dark room with a black cloth. It was found that using PMT dark noise hits for gain and SPE resolution measurements was the optimal choice. Before collecting test data, the PMTs were placed in the dark room and powered at their working HV for more than eight hours to reduce and stabilize the DCRs. Forced trigger mode (pedestal mode) was used in the tests to establish the baseline level of each channel. Subsequently, self-triggered mode was utilized to capture the SPE signals generated by PMT dark count events, with a trigger threshold set at 870 digital to analog converter units (ADCu), corresponding to about 0.3 PE.

Figure 14 and Fig. 15 show the pedestal and SPE distributions for a group of 16 PMTs, respectively. By fitting these distributions with Gaussian functions, the analog to digital converter units (ADCu) corresponding to their peak positions can be determined, referred to as Q_0 and Q_1 , respectively. Additionally, the sigma value of the Gaussian function is denoted as σ_1 for the SPE distribution. Consequently, the gain of each PMT can be calculated using the following formula:

$$\text{Gain} = \frac{Q_1 - Q_0}{1.6 \times 10^{-7} \times P_1}, \quad (2)$$

where P_1 is the calibration constant of each CATIROC channel, which is $160 \sim 190$ ADCu/pC for a CATIROC preamplifier gain of 40. As a result, the estimated range for the ΔADC value ($Q_1 - Q_0$) corresponding to a 3×10^6 gain is approximately from 77 ADCu to 91 ADCu.

In the analysis of the test data, to facilitate the comparison and evaluation of gain consistency within the same group of PMTs under a specified working HV, the average gain of the group was normalized to 3×10^6 . The gains of PMTs in the same group were scaled by the same normalization factor. Subsequently, PMTs that did not meet the acceptance criteria (gain below 2×10^6 or above 5×10^6) were excluded and replaced with spare PMTs that aligned with the working HV.

The gain distribution of the measured PMTs as obtained from this analysis is shown in Fig. 16a. The results presented in Fig. 16b demonstrate that the gain spread remains consistently around $\sim 10\%$ across different HV levels.

In addition, the SPE resolution was obtained as follows:

$$\text{SPE resolution}(\%) = \frac{\sigma_1}{Q_1 - Q_0} \times 100\% \quad (3)$$

The SPE resolution results are presented in Fig. 17, indicating that the majority of PMTs exhibit a value below 45%, thereby satisfying the acceptance criteria. The SPE resolution was further compared with the results of the bare tube tests, and good consistency was observed.

Another important acceptance parameter is the DCR, which is measured by the threshold scanning method. In this test, the number of trigger signals from each PMT channel in an electronics time period of

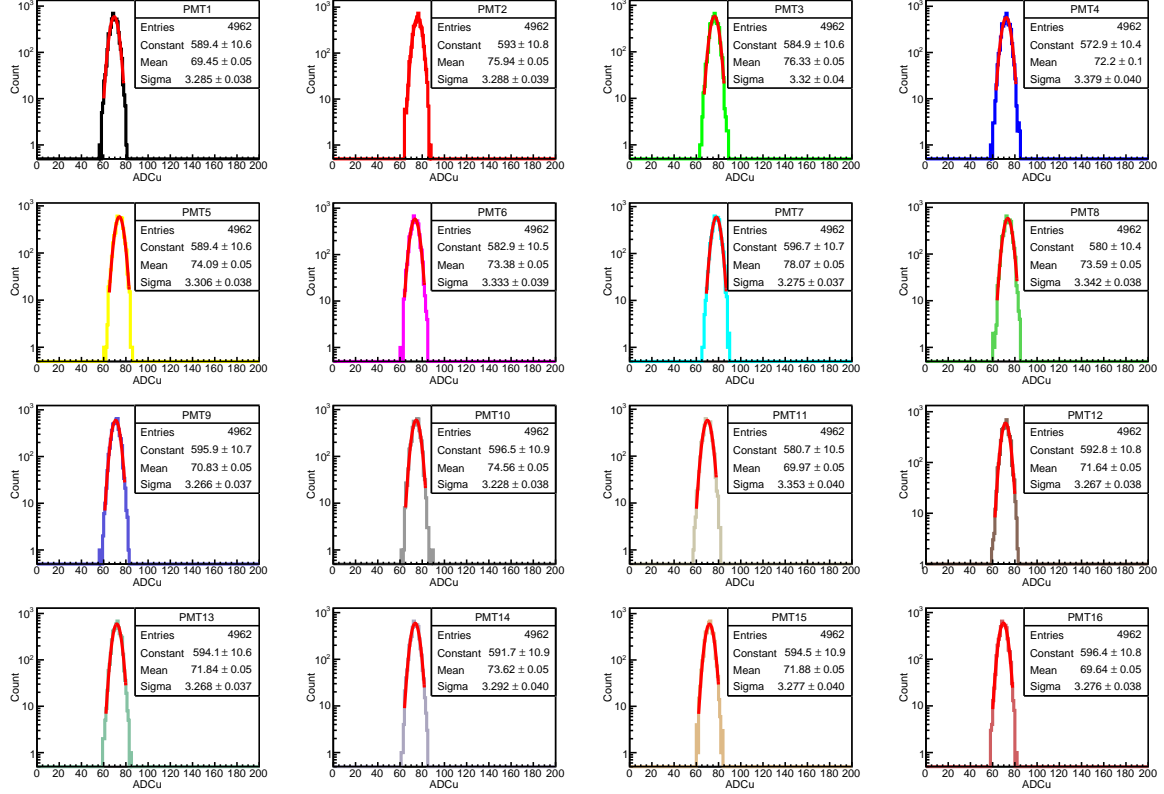


Figure 14: Pedestal charge spectra of a group of PMT.

0.419 s is measured as a function of the trigger threshold in DAC units ranging from 0 to 870. The trigger values are in inverse order: a high DACu value corresponds to a low trigger threshold value in amplitude. The counts versus the discriminator threshold (also called S-curve) is shown in Fig. 18. The PMT DCR was obtained by calculating the trigger rate at threshold 870 DACu, which corresponds to ~ 0.3 PE. Figure 19 shows the DCR distribution of the potted PMTs and the bare PMTs. The average DCR for the bare PMTs is approximately 510 Hz, with a significant tail in the distribution primarily attributed to insufficient time spent in the dark room under high voltage (HV) for the DCR to stabilize before testing. For instance, some PMTs were only subjected to a 2-hour HV load, and a DCR value below 3 kHz was considered acceptable. The potted PMTs benefited from sufficient cooling time with working HV of 8 hours, resulting in a significant reduction in the tail component and an average dark count rate of approximately 420 Hz, lower than that observed for the bare PMT test in HZC. However, upon comparing the main peak position of the dark count rate distribution, a significant shift is observed in the acceptance test, with the peak position approximately 100 Hz higher than that in the bare PMT test. Our investigation reveals that this additional contribution primarily comes from fluorescence emitted by the packaging foam employed to protect the PMTs. Subsequent tests conducted on small batches of PMTs demonstrated a difference of around 100 Hz in dark count rates between foam-protected and non-foam conditions. Given that the primary objective of the acceptance test is to validate the functionality of the potted PMTs, it was deemed unnecessary to conduct extensive testing without foam protection in order to ensure efficiency and prevent any damage during this process.

In total, 25,744 instrumented PMTs, corresponding to 1,609 groups, were tested. The rejected ratio of the acceptance test is about 0.7%. Table 4 summarizes the number of unqualified PMTs and the issues identified during testing. PMTs that did not pass the tests were removed and replaced with spare PMTs.

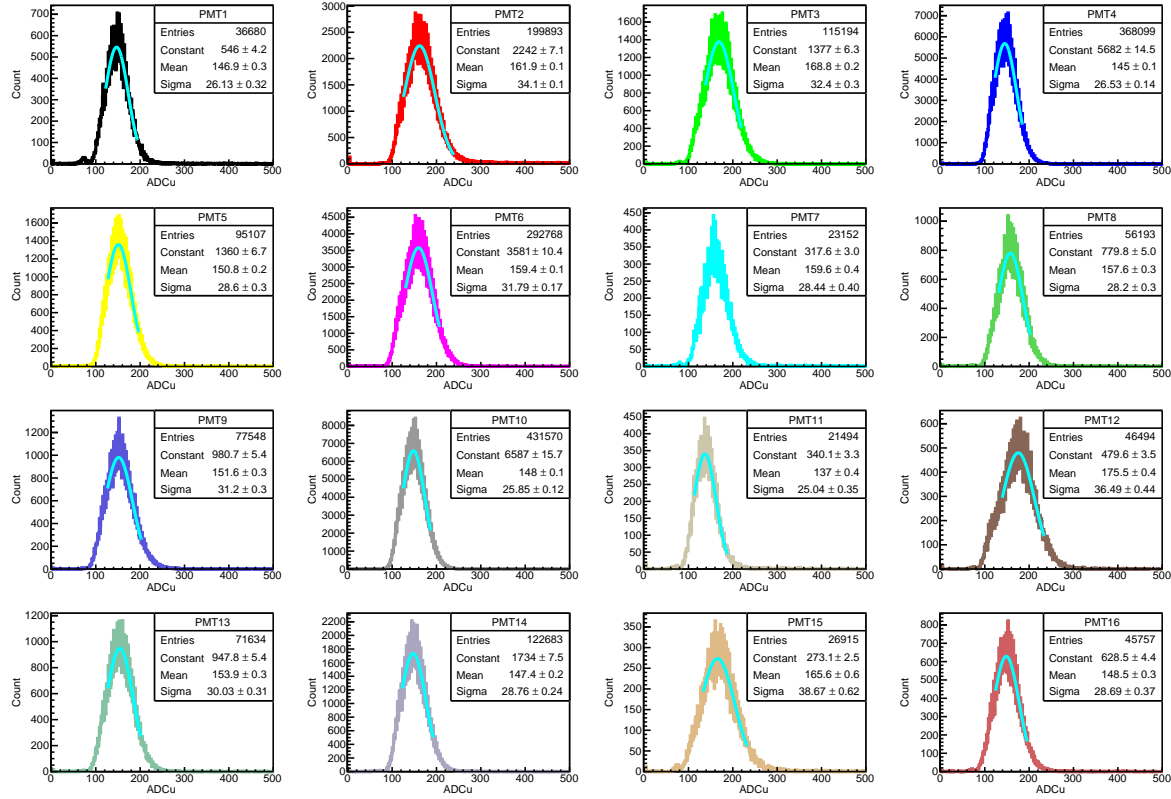


Figure 15: The SPE charge spectra of a group of PMTs.

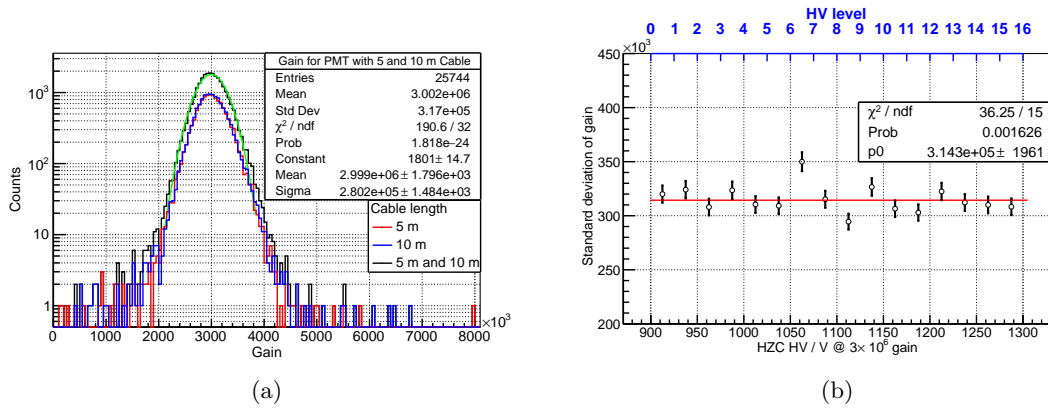


Figure 16: (a) Gain distribution of the measured PMTs. (b) Gain spread of PMTs across the 16 HV levels. The red line represents a constant fit to all points, illustrating that the spread remains consistently around $\sim 10\%$ across all HV levels.

The replaced PMTs were subsequently tested at the JUNO site, where they all met the acceptance criteria.

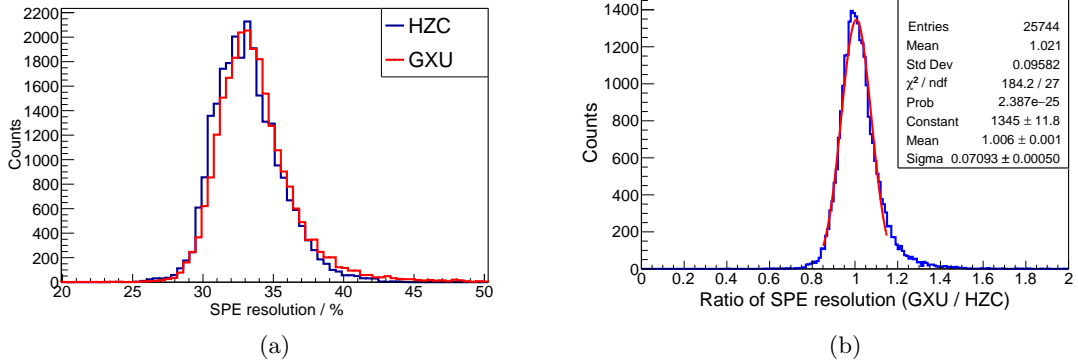


Figure 17: (a) The SPE resolution of the measured PMTs. (b) The comparison of SPE resolution between the potted PMTs and the bare PMTs.

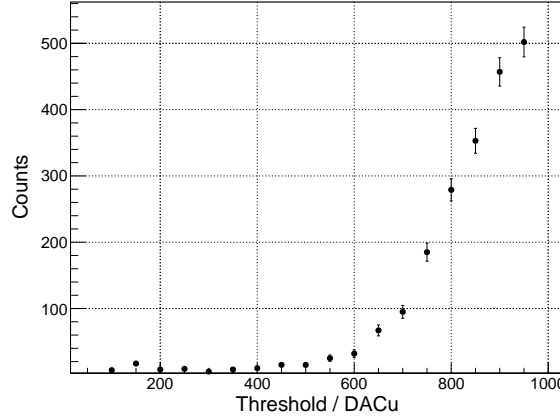


Figure 18: The S-curve for one PMT. The number of triggers counted in 0.419 s as a function of the trigger threshold in DAC unit (a high DACu value corresponds to a low trigger threshold value in amplitude).

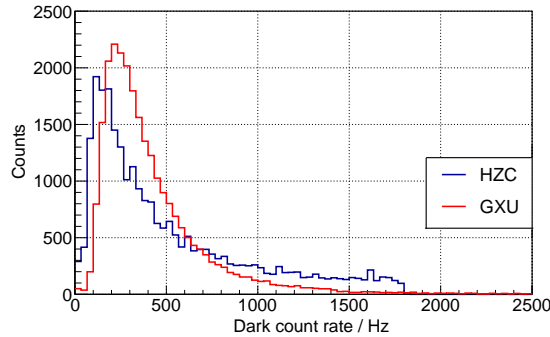


Figure 19: PMT dark rate distributions measured at the company (HZC) and during the acceptance tests at Guangxi University (GXU).

Table 4: The result of acceptance test.

| Issue | Unqualified num. |
|-------------------------------------|------------------|
| Gain + Resolution + Dark count rate | 1 |
| Gain + Resolution | 14 |
| Gain + Dark count rate | 0 |
| Resolution + Dark count rate | 0 |
| Gain | 58 |
| SPE resolution | 14 |
| Dark rate | 81 |
| Short-circuit | 9 |
| Total | 177 |

6 Summary

The instrumentation of the 3-inch PMTs of JUNO underwent rigorous testing at every stage of development and mass production. Each PMT was equipped with a divider capable of supplying up to 1,300 V across the various dynodes. Capacitors with wires and surface-mounted resistors were meticulously chosen to meet space constraints while ensuring reliability. A standard RG178 coaxial cable, available in 5 m or 10 m lengths, was used to transmit both HV and the signal. The cable jacket was customized to enhance waterproofing. A 16-channel waterproof connector, developed in collaboration with the Axon' cable company, served as the interface between the PMTs and the electronics. Signal attenuation in the cable was adequately compensated by the voltage, and the observed analog crosstalk was below 0.3%. Two long-term underwater validations were conducted, demonstrating promising reliability with FIT values of less than 500 and 350, respectively, in line with JUNO's requirements.

To integrate PMTs with HV dividers, cables, and connectors, the PMTs were grouped into more than 1,600 sets based on their weights and operating HV. Each group was connected to a single connector and arranged in the water pool from shallow to deep, according to weight, from lightest to heaviest. Waterproof potting of the PMTs was achieved through multiple redundant layers of sealants with mechanical support. A random selection of 217 groups was tested underwater, and no leakage was found in the PMT sealing.

All potted PMTs were tested with an early version of the electronics system. The SPE spectrum of each group was verified under the nominal threshold. A 10% standard deviation from the nominal 3×10^6 gain was found. After potting, the SPE resolution remained unchanged, and there was no significant variation in the DCR. Only 0.7% of potted PMTs were replaced due to high DCRs, significant deviations from the target gain, poor charge resolution, or electrical short circuits. Altogether, 25,600 instrumented PMTs, along with an additional 144 spares, were delivered to JUNO.

7 Acknowledgement

We are grateful for the ongoing cooperation from the China General Nuclear Power Group. This work was supported by the Chinese Academy of Sciences, the National Key R&D Program of China, the Guangdong provincial government, and the Tsung-Dao Lee Institute of Shanghai Jiao Tong University in China, the Institut National de Physique Nucléaire et de Physique de Particules (IN2P3) in France, the Istituto Nazionale di Fisica Nucleare (INFN) in Italy, the Fond de la Recherche Scientifique (F.R.S-FNRS) and the Institut Interuniversitaire des Sciences Nucléaires (IISN) in Belgium, the Conselho Nacional de Desenvolvimento Científico e Tecnológico in Brazil, the Agencia Nacional de Investigacion y Desarrollo and ANID - Millennium Science Initiative Program - ICN2019.044 in Chile, the European Structural and Investment Funds, the Czech Ministry of Education, Youth and Sports and the Charles University Research Center in Czech Republic, Deutsche Forschungsgemeinschaft (DFG), the Helmholtz Association, and the Cluster of Excellence PRISMA+ in Germany, the Joint Institute of Nuclear Research (JINR) and Lomonosov Moscow State University in Russia, MOST and MOE in Taipei, the Program Management Unit for Human Resources & Institutional Development, Research and Innovation, Chulalongkorn University, and Suranaree University of Technology in Thailand, the Science and Technology Facilities Council (STFC) in the UK, University of California at Irvine and the National Science Foundation in the US.

References

- [1] JUNO, F. An *et al.*, Neutrino Physics with JUNO, *J. Phys. G* **43**, 030401 (2016), arXiv:1507.05613.
- [2] JUNO, Z. Djurcic *et al.*, JUNO Conceptual Design Report, (2015), arXiv:1508.07166.
- [3] JUNO, A. Abusleme *et al.*, JUNO physics and detector, *Prog. Part. Nucl. Phys.* **123**, 103927 (2022).
- [4] JUNO, A. Abusleme *et al.*, The design and technology development of the JUNO central detector, *Eur. Phys. J. Plus* **139**, 1128 (2024), arXiv:2311.17314.
- [5] JUNO, A. Abusleme *et al.*, Mass testing and characterization of 20-inch PMTs for JUNO, *European Physical Journal C – Particles & Fields* **82** (2022).
- [6] C. Cao *et al.*, Mass production and characterization of 3-inch PMTs for the JUNO experiment, *Nucl. Instrum. Meth. A* **1005**, 165347 (2021), arXiv:2102.11538.
- [7] JUNO, A. Abusleme *et al.*, Calibration Strategy of the JUNO Experiment, *JHEP* **03**, 004 (2021), arXiv:2011.06405.
- [8] A. Cabrera *et al.*, Multi-calorimetry in light-based neutrino detectors, *JHEP* **12**, 002 (2024), arXiv:2312.12991.
- [9] JUNO, A. Abusleme *et al.*, Prediction of Energy Resolution in the JUNO Experiment, *Chin. Phys. C* **49**, 013003 (2025), arXiv:2405.17860.
- [10] S.-Y. Zhang, Y.-B. Huang, M. He, C.-F. Yang, and G.-M. Chen, Sub-GeV events energy reconstruction with 3-inch PMTs in JUNO, *Nucl. Sci. Tech.* **36**, 84 (2025), arXiv:2402.13267.
- [11] C.-F. Yang *et al.*, Reconstruction of a muon bundle in the JUNO central detector, *Nucl. Sci. Tech.* **33**, 59 (2022), arXiv:2201.11321.
- [12] JUNO, A. Abusleme *et al.*, JUNO Sensitivity on Proton Decay $p \rightarrow \bar{\nu}K^+$ Searches, *Chin. Phys. C* **47**, 113002 (2023), arXiv:2212.08502.
- [13] JUNO, A. Abusleme *et al.*, Sub-percent precision measurement of neutrino oscillation parameters with JUNO, *Chin. Phys. C* **46**, 123001 (2022), arXiv:2204.13249.
- [14] JUNO, S. Conforti *et al.*, CATIROC: an integrated chip for neutrino experiments using photomultiplier tubes, *JINST* **16**, P05010 (2021), arXiv:2012.01565.
- [15] P. Walker *et al.*, The High Voltage Splitter board for the JUNO SPMT system, *Nucl. Instrum. Meth. A* **1082**, 171022 (2025), arXiv:2505.05586.
- [16] G. Wang, Effect of divider current on 7.62 cm photomultiplier tube performance (in chinese), *Nuclear Techniques* **41** (2018).
- [17] G. Wang, Design and study of 3-inch pmt's hv divider for juno (in chinese), Master's thesis, Nanhua University, 2018.
- [18] C. Cao, *The small PMT performance and related physics study in JUNO (in Chinese)*, PhD thesis, University of Chinese Academy of Sciences, 2021.
- [19] <https://www.nextpcb.com/blog/guide-to-fr-4-printed-circuit-board-material-nextpcb>,
<https://resources.altium.com/p/fr4>,
<https://www.pcbelec.com/pcb-materials/fr4-material>.

- [20] JUNO, A. Abusleme *et al.*, Radioactivity control strategy for the JUNO detector, *JHEP* **11**, 102 (2021), arXiv:2107.03669.
- [21] A. Yang *et al.*, Study and removal of the flash from the HV divider of the 20-inch PMT for JUNO, *JINST* **15**, T04006 (2020).
- [22] N. Li *et al.*, Characterization of 3-inch photomultiplier tubes for the JUNO central detector, *Radiation Detection Technology and Methods* **3**, 6 (2019).
- [23] D. Wu, J. Xu, M. He, Z. Wang, and Z. Chu, Study of the front-end signal for the 3-inch PMTs instrumentation in JUNO, *Radiat. Detect. Technol. Methods* **6**, 349 (2022), arXiv:2204.02612.
- [24] <https://www.viking.com.tw/>.
- [25] <https://www.murata.com/products/capacitor>.
- [26] <https://www.axon-interconnect.com/>.
- [27] S. O. Flyckt and C. Marmonier, *Photomultiplier Tubes: Principles and Applications*, 2nd ed. (Photonis, Brive, France, 2002), https://www2.pv.infn.it/~debari/doc/Flyckt_Marmonier.pdf.
- [28] D. Wu *et al.*, Study on the linearity of 20" dynode and MCP PMTs, *JINST* **18**, P05033 (2023), arXiv:2212.11514.
- [29] <https://www.keysight.com/us/en/assets/9018-04906/installation-guides/9018-04906.pdf>.
- [30] Z. Chu *et al.*, A highly sensitive SF₆-based leak test system for JUNO 3-inch PMT underwater electronics boxes, (2025), arXiv:2505.24142.
- [31] S. P. Timoshenko and J. M. Gere, *Theory of Elastic Stability*, 2 ed. (McGraw Hill, New York, 1961).
- [32] <https://www.vitalchem.com/>.